

Source separation algorithms applied to magnetoencephalographic signals

Giulia Barbati^{1,2}, Camillo Porcaro^{2,3}, Filippo Zappasodi^{4,2}, Franca Tecchio^{4,2}

¹ Department of Public Health and Microbiology, University of Turin, Italy

² AFaR, Centre of Medical Statistics & IT, Fatebenefratelli Hospital, Rome, Italy

³ ITAB – Institute for Advanced Biomedical Technologies, “G. D’Annunzio” University, Chieti, Italy

⁴ ISTC – Institute of Science and Technologies of Cognition, CNR, Rome, Italy

Corresponding Author:

Giulia Barbati, Department of Public Health and Microbiology

Via Santena 5 bis, 10126 Torino, Italy

E-mail: giulia.barbati@unito.it

Summary

Physiological activity in the brain can be evaluated by means of non-invasive electrophysiological techniques like electroencephalography (EEG), and magnetoencephalography (MEG): such instruments are able to obtain cerebral processing measures with optimal time resolution. The crucial problem is then to gain access to the inner neural code starting from extra-cranial recordings: cerebral signals related to significant activity are mixed and embedded in unstructured noise and in other physiological artefacts, not relevant to the desired observation.

To deal with this problem, a statistical-based approach has recently been introduced based on the exploitation of statistical properties of sources comprised in the observed signals without any assumption about the biophysical model underlying the recorded signals. In particular, the “Independent Component Analysis” (ICA) model assumes that sources are statistically mutually independent; to extract them from the mixture a measure of non-Gaussianity is maximised (i.e. kurtosis).

In this paper, we discuss how the ICA assumptions fit with the complex and interconnected activity of cerebral networks activity and we describe our newly proposed “Functional Source Separation” (FSS) algorithm, conceived as a generalisation of the basic ICA model. Some physiological constraints, according to the expected temporal behaviour of the cerebral sources of interest, are added to the maximisation of kurtosis producing a multi-objective cost function that exploits global statistical features and functional source properties simultaneously. Some of the ICA and FSS applications from our previous studies are reviewed and discussed in order to provide application examples.

Our conclusions are that the ICA algorithm could be successfully applied for specific issues, such as artefact removal, but the proposed multi-objective FSS cost function provides a more general framework for estimating cerebral activity of interest.

KEY WORDS: *Blind Source Separation (BSS), Independent Component Analysis (ICA), Functional Source Separation (FSS), Magnetoencephalography (MEG).*

Introduction

When studying cerebral activity through neurophysiological techniques – such as electroencephalography (EEG) and magnetoencephalography (MEG) – the main goal is the discrimination of different sources of electrical activity. The first step in this direction is to separate the “cerebral” activity from “other activity”, generated by non-cerebral sources, the latter often being of such intensity that the former is hidden. Typically, a MEG system measures the mixture of original source signals and additive noise

(1): this mixture derives from both the “wanted” sources and those that are “to be discharged” (called artefacts).

The Independent Component Analysis (ICA) technique can be useful for the elimination of artefacts and noise from biomedical signals; the theory of the ICA algorithm was described systematically for the first time in (2), and has been widely applied to the analysis of cerebral signals in the past decade, starting from the first application to EEG signals by Makeig and colleagues (3). The basic assumption of ICA is that a set of statistically independent sources \mathbf{S} has been

mixed linearly in the observed data \mathbf{X} by means of an unknown mixing matrix \mathbf{A} . The aim is to recover both \mathbf{S} and \mathbf{A} starting from the observation of the linear mixture $\mathbf{X}=\mathbf{AS}$, without making any particular assumption other than that of the statistical independence of the sources. ICA could be viewed as a development of the classic statistical technique of “Principal Component Analysis” (PCA) (4): given a set of multivariate measurements, the purpose of PCA is to find a smaller set of variables with less redundancy, that would give as good a representation as possible. In PCA, the redundancy is measured by correlations between data elements, while in ICA the much richer concept of independence is used, and less emphasis is placed on the reduction of the number of variables. In the context of signal processing, both these methods are comprised in the general family of the “Blind Source Separation” (BSS) techniques. ICA has been applied not only for removing artefacts from electrophysiological signals, but also for estimating cerebral activity involved in particular tasks (5). An important debate has arisen among neuroscientists on the appropriateness of the ICA model in describing cerebral network activity.

The aim of the present paper is to discuss this point, by means of an ad hoc review of some representative ICA applications performed in our MEG laboratory both on cerebral signals and foetal cardiac heartbeat detection. On the basis of the results that emerged from those studies, we explain the reason we proposed a new algorithm called “Functional Source Separation” (FSS) (6-9). It adds a functional task-related reactivity constraint to the cost function of the ICA model, i.e. the ‘responsiveness’ to a specific task performed by the subject during the experiment is maximised; the functional constraint is based on a priori knowledge of the cerebral reaction to the task under observation. Two applications of this algorithm are described, in which FSS was compared to ICA and PCA performances on the basis of the functional activation properties of the extracted sources and their estimated spatial positions on the cortical surface.

Applications of ICA to MEG data

Independent Component Analysis is a generative ‘latent variables’ model that describes how the ob-

served data are generated by a process of mixing the underlying unknown sources. The set of recorded signals \mathbf{X} is assumed to be obtained as a linear combination (through an unknown mixing matrix \mathbf{A}) of statistically independent non-Gaussian sources \mathbf{S} (at most one Gaussian): $\mathbf{X}=\mathbf{AS}$. Sources \mathbf{S} are estimated (taking account of arbitrary scaling and permutations) by independent components \mathbf{Y} as: $\mathbf{Y}=\mathbf{WX}$, where the unmixing matrix \mathbf{W} is estimated along with the components. The basic estimation idea of ICA is that, according to the central limit theorem, sums of non-Gaussian independent random variables are closer to a Gaussian than the original variables. Therefore, if we take a linear combination $y = \sum_i w_i x_i$ of the observed mixture variables (which, because of the linear mixing model, is a linear combination of the independent components as well), this will be maximally non-Gaussian if it equals one of the independent components. Thus, the first ICA ‘estimation principle’ can be stated as follows: “find the local maxima of non-Gaussianity of a linear combination $y = \sum_i w_i x_i$ under the constraint that the variance of y is constant. Each local maximum gives one independent component”. Moreover, since independence implies (non-linear) uncorrelatedness, the second ICA ‘estimation principle’ could be formulated as: “find the matrix \mathbf{W} so that for any $i \neq j$, the components y_i and y_j are uncorrelated, and the transformed components $g(y_i)$ and $h(y_j)$ are uncorrelated, where g and h are suitable non-linear functions”. Therefore the goal of ICA is to determine a transformation which assures that the output signals are as independent as possible. Technical details of the ICA algorithms can be found in (10, 11).

ICA for artefact identification and removal from MEG signals

In the application to MEG data, \mathbf{X} represents the matrix of the recorded signals: a MEG system has a certain number m of sensors (m could vary from 20 to 500 sensors, depending on the system), positioned over the subject’s head, and the magnetic fields generated by the subject’s brain activity are recorded for a number T of time points. Therefore, the \mathbf{X} matrix has as many rows as the number of sensors (m , the number of MEG channels) and as many columns as the time samples (T , depending on the sampling frequency: generally, this is 1000 Hz, so that one minute

of recording=60000 sample points). When ICA is applied to the \mathbf{X} matrix, the output of the algorithm is a \mathbf{Y} matrix $m \times T$, where each row represents an estimated independent component (IC) of the same dimension as the original channels (rows of \mathbf{X}) and the estimate of the separating \mathbf{W} matrix of dimension $m \times m$. It is therefore necessary to examine visually the time courses of each IC, together with its weights on the original sensors – the corresponding column of \mathbf{W} , the so-called IC ‘topography’ on the scalp – and decide which is representing cerebral activity and which could be discarded as ‘artefact’ and noise. In our first application of ICA (12), we developed a procedure to detect the ICs to be discharged as artefacts: in brief, the outputs of the ICA algorithm pass through a detection system which takes the decision to reject or to retain the given IC. Four markers are considered for artefact recognition: percentage of kurtosis-outlier segments, global kurtosis coefficient, percentage of entropy-outlier segments (all based on IC statistical properties), and correlation coefficient with Power Spectrum Density (PSD) of typical artefacts (based on IC spectral characteristics). For each IC, the detection system takes the reject decision when at least one of these criteria is fulfilled. Then, the retained ICs, denoted as $\hat{\mathbf{y}}_k$ ($k \leq m$), pass through the inverse system represented by the inverse \mathbf{W}^+ of

the estimated separation matrix thereby reconstructing data: $\mathbf{x}_{\text{Rec}}^{\mathbf{p}} = \mathbf{W}_k^+ \hat{\mathbf{y}}_k$; the superscript \mathbf{p} shows that a part of the original signals could not be explained by the selected ICs and \mathbf{W}_k^+ denotes the corresponding selected k columns of \mathbf{W}^+ . We then define a measure of ‘discrepancy’ as the difference between the original data and the retro-projected ones:

$$\mathbf{d} = \mathbf{x} - \mathbf{x}_{\text{Rec}}^{\mathbf{p}} = \mathbf{x} - \mathbf{W}_k^+ \mathbf{W}_k \mathbf{x} = [\mathbf{I} - \mathbf{W}_k^+ \mathbf{W}_k] \mathbf{x} \quad (1)$$

To verify and possibly improve the performance of the retro-projection process, we carry out a control cycle by examining the spectral characteristics of the m -dimensional discrepancy vector. At the end of this process we obtain the final m -dimensional vector of the reconstructed sensor signals $\mathbf{x}_{\text{Rec}}(t) = [x_{\text{Rec}_1}(t), \dots, x_{\text{Rec}_m}(t)]^T$. As shown in Figure 1, panel (a), ICs corresponding to typical artefacts such as ocular movements, cardiac heartbeat and power line noise, are characterised by high absolute kurtosis values (for Gaussian signals kurtosis is zero), respectively indicating super-Gaussian (ocular/cardiac) and sub-Gaussian (power line noise) behaviours. For this reason, the ICA algorithm is particularly effective in detecting these types of signal. In panel (b) of Figure 1, the data cleaning procedure is illustrated: the original MEG channels, contaminated by artefacts, are reconstructed by dis-

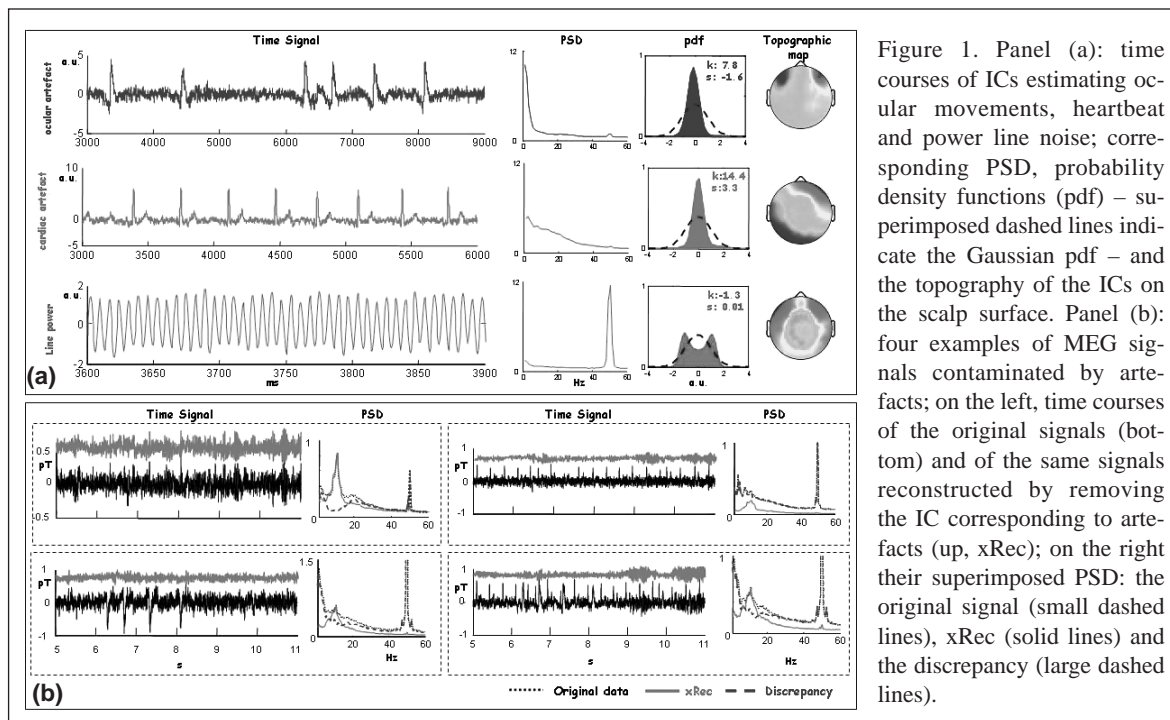


Figure 1. Panel (a): time courses of ICs estimating ocular movements, heartbeat and power line noise; corresponding PSD, probability density functions (pdf) – superimposed dashed lines indicate the Gaussian pdf – and the topography of the ICs on the scalp surface. Panel (b): four examples of MEG signals contaminated by artefacts; on the left, time courses of the original signals (bottom) and of the same signals reconstructed by removing the IC corresponding to artefacts (up, xRec); on the right their superimposed PSD: the original signal (small dashed lines), xRec (solid lines) and the discrepancy (large dashed lines).

charging the ICs corresponding to artefacts. In this way, the obtained 'xRec' (cleaned MEG signal) contains only the cerebral frequencies of interest, and the residual discrepancy captures artefacts and noise.

ICA applied to foetal magnetic recordings

Foetal magnetocardiography (fMCG) (13, 14) is a non-invasive technique used for the assessment of foetal heart functions and well being in a variety of clinical situations (15). fMCG recordings could be viewed as mixtures of signals related to foetal cardiac activity, maternal cardiac function and environmental magnetic noise. The detection of foetal cardiac signals from fMCG data is very difficult, since the foetal heartbeat has a much smaller magnitude than the maternal heartbeat at all gestational ages and can be almost completely hidden by noise during early gestation. In addition, the foetal and maternal cardiac sources almost overlap in the time/frequency domain. The rationale of applying ICA to fMCG data is that signals detected by the MEG sensors positioned over the mother's abdomen are considered as

a linear mixture of stochastically independent contributions coming (i) from the foetal heartbeat, which is what we want to investigate, (ii) from unwanted biological near-field sources, as for example, the maternal heartbeat, or gastric and uterine muscle contractions, motion artefacts, etc., and (iii) from the external environment.

Given these properties, we deemed it reasonable to apply ICA for foetal heartbeat signal extraction (16). fMCG data were recorded from 12 pregnant women using a 25-sensor array placed over the mother's abdomen. To have a reference for the maternal cardiac signal, an electrocardiogram (ECG) of the mother was simultaneously acquired. In all 12 recordings, the ICA algorithm successfully extracted ICs that could be clearly associated with cardiac sources. We used spectral coherence (i.e. correlation in the frequency domain) between ICs and recorded traces to safely discriminate maternal from foetal components. Although signals generated by the mothers' hearts generally dominated the recorded traces, the amplitudes showed fetus/mother ratios that varied

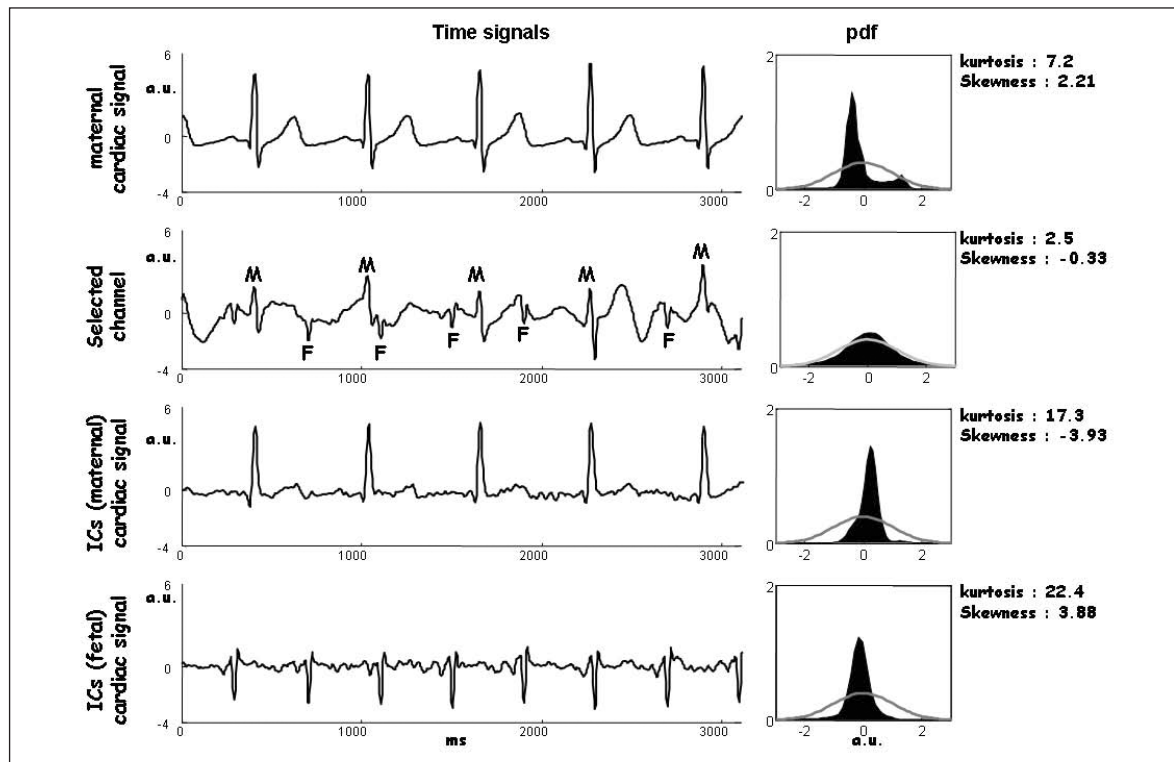


Figure 2. Left: Maternal cardiac signal measured by the electrocardiogram (ECG); a selected fMCG channel with the maternal and foetal heart beats mixed (indicated respectively as M and F); IC corresponding to the maternal heartbeat; IC corresponding to the foetal heartbeat. Right: Corresponding probability density functions (pdf) of the signals with their kurtosis/skewness values (superimposed lines indicate the Gaussian pdf).

from case to case, most likely due to the different foetal positions with respect to the sensors array. Figure 2 shows some of the results obtained: the ICA algorithm successfully estimated the foetal heartbeat, by exploiting the super-Gaussian characteristics of this signal with respect to the original recorded mixture, in spite of the smaller magnitude of the foetal heartbeat with respect to the maternal one.

The application of ICA to detect functionally different intra-regional neuronal pools

In a subsequent study, we investigated whether ICA was able to identify different cerebral sources and whether it was possible to significantly differentiate these estimated sources by exploiting directly their task-related behaviour. Cerebral activity was recorded during a simple motor task, in five subjects, each one repeated five times on different days. The subjects were required to alternate a rest state (*relaxation*) to the simple hand opening-closing (*movement*). Estimated ICs were flagged through a clustering procedure based on a functional task-related measure. Intra-subject inter-session repeatability and functional differences of obtained IC clusters were tested to assess the statistical significance of the procedure (17). Kurtosis levels of the estimated ICs were computed and compared between the functionally labelled IC sources and the ICs marked as artefacts. Since neuronal area involvement in the selected task could be assessed from activity reduction between the *movement* and *relaxation* states, mostly in the *alpha* (α : [7.5-12.5] Hz) and *beta* (β : [13-25] Hz) frequency bands – a phenomenon called ‘event-related desynchronisation’ – the following reactivity measure was used:

$$react(\hat{y}_k^j)_{\alpha,\beta} = \frac{PSD(\hat{y}_k^j)_{\alpha,\beta}^{relax} - PSD(\hat{y}_k^j)_{\alpha,\beta}^{movement}}{PSD(\hat{y}_k^j)_{\alpha,\beta}^{relax}} \quad (2)$$

where \hat{y}_k^j is the k^{th} IC of the j^{th} session of the subject, and the PSD difference is computed between relax and movement conditions in the α and β bands and normalised to the corresponding PSD level in the relaxation state. Using this reactivity index, for each subject we clustered the ICs corresponding to the activated cerebral sources, defining as *Mu* the group of ICs with the greatest reactivity index, and as *Alpha* the ICs in the second cluster, in decreasing order of

reactivity. As depicted in Figure 3, across subjects and sessions, kurtosis was significantly lower for *Mu* and *Alpha* ICs with respect to ICs marked as *Artefacts*, and was not significantly different between *Mu* and *Alpha* (*Artefacts* versus *Mu*, $p=0.002$, *Artefacts* versus *Alpha*, $p=0.007$, *Mu* versus *Alpha*, $p>0.6$, ANOVA test corrected for multiple comparisons). As expected, the reactivity index was significantly higher for *Mu* and *Alpha* sources with respect to *Artefacts*, respectively $p<0.0001$ and $p=0.03$, and was significantly higher for *Mu* versus *Alpha* ($p<0.0001$). Kurtosis was inversely associated with reactivity (Pearson’s $r = -0.23$, $p=0.008$): ICs corresponding to the event-related desynchronisation phenomena thus appeared therefore as the ‘residual’ ones in the ICA estimation procedure.

Therefore, while the ICA non-Gaussianity assumption was found to be in agreement with the characteristics of the most common artefacts, like heartbeat and ocular movements, as shown in panel (a) of Figure 1, and the required independence with respect to the underlying brain activity could easily be justified, the same estimation principle seemed to disagree somewhat with the characteristics of the cerebral sources of interest: the reactivity criterion used to identify sources were found to be inversely associated with the non-Gaussianity index of kurtosis.

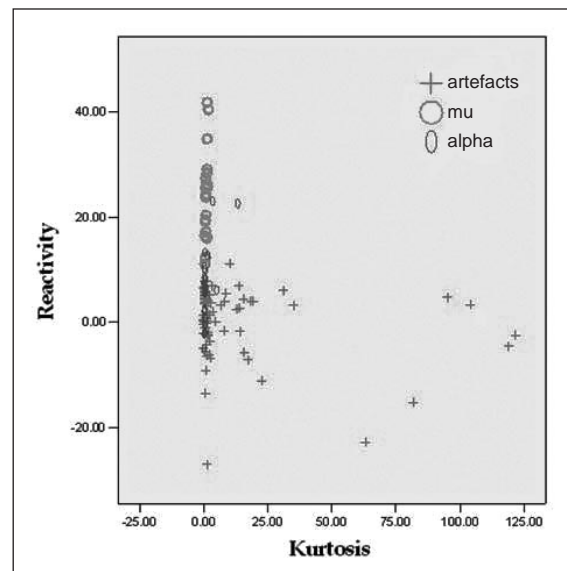


Figure 3. Scatter plot of the reactivity index versus kurtosis for the ICs corresponding to *Alpha* (ovals), *Mu* (circles), and for ICs marked as *artefacts* (crosses), across subjects and sessions.

These results suggested a possible way of improving sources separation: by adding some event-related functional constraints directly to the algorithm's cost function.

Functional Source Separation applied to MEG data

As in the ICA model, FSS starts from an additive, hidden linear mixture of sources $\mathbf{X}=\mathbf{A}\mathbf{S}$, where \mathbf{X} represents the observed data, \mathbf{S} the underlying unknown sources, and \mathbf{A} the source-sensor coupling matrix to be estimated. Additional information is used to bias the decomposition algorithm towards solutions that satisfy physiological assumptions, by means of a multi-objective cost function: $F = J + \lambda R$, where J is the non-Gaussianity measure generally used in ICA (for example kurtosis), λ is a parameter to weigh the two parts of the contrast function, and R accounts for the prior information used to extract sources. If λ is set to zero, maximisation of F leads to the ICA model. The value of this tuning parameter has to be selected according to the data. FSS therefore exploits global statistical features (J) and functional properties of the source of interest (R) simultaneously. To separate contributions representing different sources, the proposed procedure could be applied in two different ways: by using an orthogonal extraction scheme, as in the basic ICA model, denoted as "Functional Component Analysis" (FCA); after having estimated the first source, the second one is searched for in the orthogonal space with respect to the first, and so on until the last component is estimated, with a stop rule that can be defined according to the data. Alternatively, the orthogonalisation step could be skipped, producing a non-orthogonal extraction scheme. In this condition, the order of extraction is not significant, because the algorithm is applied to the original data each time; clearly, different constraints have to be applied each time to produce different sources. Optimisation is performed by simulated annealing (18), so that the cost function can have any form (e.g. it does not need to be differentiable) and, if the algorithm is properly set, a global maximum is reached. Details on the optimisation technique can be found in (6).

FSS applied to evoked responses. In the first FSS application (6), a very simple experiment was considered: in 15 subjects MEG cerebral activity was recorded during separate little finger, thumb and median nerve galvanic stimulation. The aim was to extract sources corresponding to single finger cortical representation during different activation states, by using a proper functional constraint. Both the proposed separation algorithm versions, FCA and FSS, were compared to a standard ICA algorithm (10). Performances were judged on the basis of spatial positions and functional activation properties of the extracted sources during the three different stimuli. To identify neural networks devoted to individual finger central representation, 'reactivity' to stimuli was taken into account. It was defined as follows: the evoked activity (EA) was computed separately for the three sensorial stimulations by averaging signal epochs centred on the corresponding stimulus (EA_L, little finger; EA_T, thumb; EA_M, median nerve). The reactivity coefficient (R_{stim}) was then computed as the difference in the average signal after the stimulus arrival with respect to the baseline:

$$R_{stim} = \int_{20}^{40} |EA_{stim}(t)| dt - \int_{-30}^{-10} |EA_{stim}(t)| dt \quad (3)$$

with $stim = T, L, M$ and $t = 0$ corresponding to the stimulus arrival. The time interval ranging from 20 to 40 ms includes the maximum activation (19), and the baseline (no response) was computed in the pre-stimulus time interval (-30 to -10 ms). In Figure 4, panel (a), the evoked activity of the finger sources (little finger and thumb) extracted by the two proposed procedures is depicted (FCA: FC_L = FS_L, FC_T – since the little finger source is the first extracted, it is the same in the FCA and FSS procedure – FSS: FS_L, FS_T) during the stimulation of the thumb (EA_T), little finger (EA_L), and median nerve (EA_M) for one subject. The selective reactivity of each finger source to the respective finger stimulation is noteworthy; moreover, the FS_T reaction to the median nerve stimulation was even higher than to the stimulation of the thumb; this behaviour is considered more 'physiological' by neurologists and was obtained from the non-orthogonal FSS extraction scheme. ICA failed to separate the two finger sources in more than half the cases – in those cases a 'mixed' source IC_{T:L} was estimated, reacting both to little finger and thumb stimulation.

FSS applied to induced responses. In another FSS application (7), the aim was to explore the performance of the algorithm in reconstructing induced activity and, thus, the modulation of ongoing brain rhythms due to external events. Although such induced activity changes are statistically robust phenomena, they are not strictly time-locked to the stimulus/task onset, and therefore do not result in a strong average evoked response. We set out to investigate whether FSS was able to describe the induced responses by reanalysing an MEG dataset of a visual spatial frequency tuning paradigm: subjects viewed a set of static square-wave grating patterns for 4.5 sec ('Task') followed by 4.5 sec of a uniform field of the same mean luminance (control condition or passive period, referred to as 'Rest'). The spatial frequency of the gratings was randomly alternated at 0.5, 3 or 6 cycles per degree (cpd) (20). FSS results were compared to PCA and ICA outputs. Principal Components (PCs) and ICs were computed in two ways: from the original MEG data matrix (cases indicated as 'PCA' and 'ICA') and from the MEG data filtered in the γ (gamma, 20-70 Hz) frequency band (cases indicated as 'PCA filt' and 'ICA filt'), in order to facilitate signal recovery. To design the task-related constraint for the FSS application, we made use of the well-documented functional aspect of a robust and temporally sustained stimulus-induced power increase of gamma activity in the visual cortex

(21). Accordingly, the following ad hoc functional constraint R was defined:

$$R(\mathbf{FS}) = \frac{\sum_{\gamma} \text{PSD}_{\text{Task}}^{\text{FS}} - \sum_{\gamma} \text{PSD}_{\text{Rest}}^{\text{FS}}}{\sum_{\gamma} \text{PSD}_{\text{Rest}}^{\text{FS}}} \quad (4)$$

by computing the PSD area difference of the source (FS) between Task and Rest in the gamma (γ : 20-70 Hz) frequency band and standardising this difference with respect to the gamma activity level at Rest. In figure 4, panel (b) up, the mean percentage of source maps in the area of interest (visual cortex) across subjects for each method is depicted; in panel (b) bottom, bars representing mean spatial frequency-related gamma reactivity indices of the selected sources across subjects for each method are shown. The superior performance of FSS over ICA and PCA in estimating the induced gamma activity in the visual cortex is clearly evident.

ICA versus FSS: non-Gaussianity and functional reactivity

As the proposed FSS procedure includes physiological constraints in the cost function, it is interesting to evaluate the trade-off between non-Gaussianity maximisation and the introduced multi-objective optimisation. For this purpose, kurtosis values of the FCA, FSS sources and the corresponding ICA components across subjects were compared.

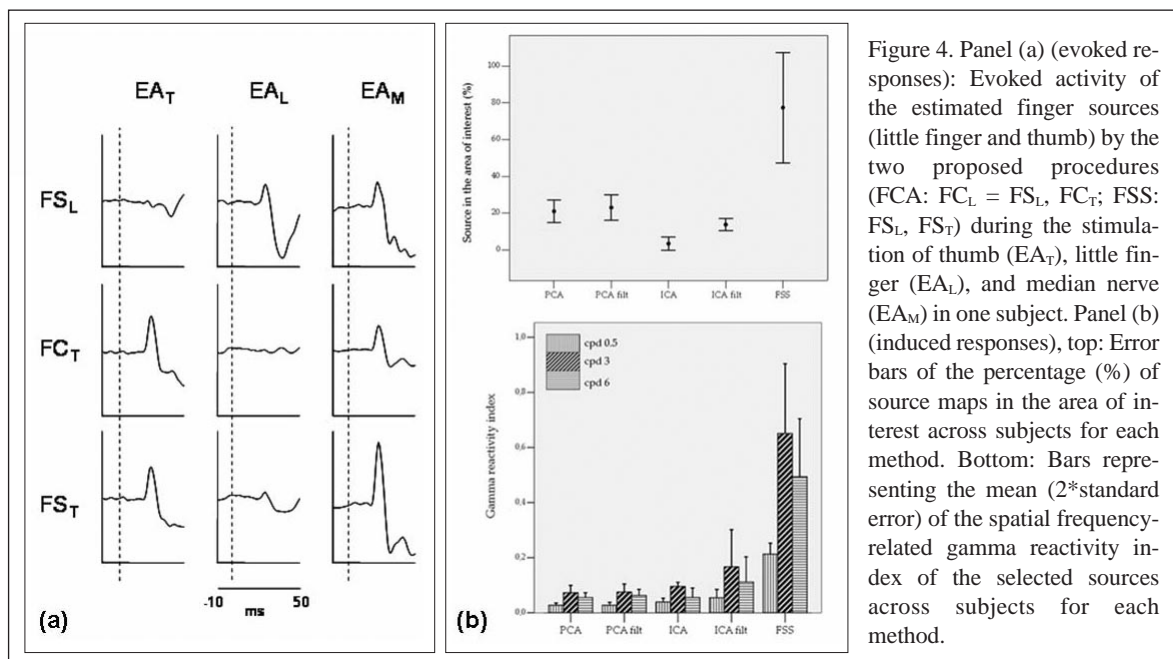


Figure 4. Panel (a) (evoked responses): Evoked activity of the estimated finger sources (little finger and thumb) by the two proposed procedures (FCA: FC_L = FS_L, FC_T; FSS: FS_L, FS_T) during the stimulation of thumb (EA_T), little finger (EA_L), and median nerve (EA_M) in one subject. Panel (b) (induced responses), top: Error bars of the percentage (%) of source maps in the area of interest across subjects for each method. Bottom: Bars representing the mean (2*standard error) of the spatial frequency-related gamma reactivity index of the selected sources across subjects for each method.

Evoked responses. When comparing the kurtosis values of FCA and FSS finger sources and the ICA ones, we found that kurtosis was significantly higher for ICA than FCA and FSS, as expected, and that these last two were not significantly different (FCA versus ICA: $p=0.03$; FSS versus ICA: $p=0.01$; FCA versus FSS: $p=0.8$; ANOVA corrected for multiple comparisons). This result was not surprising, due to the introduction of the functional constraint in FCA and FSS in addition to the kurtosis maximisation. An interesting finding was obtained when comparing kurtosis values between finger sources and ‘residual components’ for FCA versus ICA. For FCA ‘residual components’ are defined as all the components extracted orthogonally to the first two, without activating the functional constraints ($\lambda=0$), and for ICA they are defined as the remaining ICs, once the components corresponding to finger activation have been selected having excluded, from both methods, artefact components showing extreme kurtosis values. In both cases, kurtosis was significantly higher for the finger evoked-response sources than for the residual components (FCA: $p=0.01$; ICA: $p<0.0001$), indicating that, in this case, non-zero kurtosis values are associated with functional source properties (kurtosis values between 3 and 4). We could not perform this check between sources and noise for the FSS procedure, since, without imposing the functional constraints and without the orthogonality condition, no further source extraction was feasible after the first two.

Induced responses. A significant inverse relationship between the kurtosis of the components and ‘good’ spatial map characteristics was present (Spearman $\rho=-0.13$, $p=0.002$), in the sense that low kurtosis values were associated with the estimated sources in the visual area. Moreover, no significant differences in kurtosis between the selected components across methods was found; kurtosis values of the retained components were about those of a Gaussian signal, with the median value equal to 0.3 (0 for the Gaussian) and the inter-quartile kurtosis range [0.13-0.5].

Conclusions

Nearly eleven years after the usefulness of ICA for EEG/MEG analysis was first discovered (3), it is in-

creasingly accepted by many researchers that ICA is an effective method for removing stereotyped data artefacts including eye blinks and lateral eye movements, muscle activities, electrode or line noise, and cardiac artefacts; in the present paper further demonstration of this property is provided, with ad hoc evaluations of the statistical characteristics of the artefact signals. Moreover, analysis of kurtosis values of the foetal MEG data showed that the ICA model could also be successfully applied for a clear separation of the baby’s from the mother’s heartbeat. Instead when an MEG study of desynchronisation in brain phenomena was analysed, the ICA model revealed an evident discrepancy with the characteristics of the functionally reacting sources; this finding prompted a new approach to the cerebral source separation problem, that we described in the second part of this paper. The novel Functional Source Separation method (FSS) was conceived as a generalisation of the basic ICA model: some physiological constraints, defined from expected temporal behaviour of the cerebral sources of interest, are added to the maximisation of kurtosis, producing a multi-objective cost function that exploits global statistical features and functional properties of the source of interest simultaneously. The relative influence of these two aspects could be adjusted on the specific dataset. Moreover, the orthogonality constraint could be removed, allowing the correlated source activity to be estimated. Results obtained in FSS applications, together with the previous ICA studies, provided material for a meta-analysis of the statistical and functional characteristics of the estimated sources across different experimental set-ups.

We conclude that for some types of source the relevant information could be effectively synthesised with a single index, computed on the (approximate) signal probability distribution, as in the case of artefacts. For evoked sources it is instead appropriate to add a functional constraint to obtain an efficient separation, even if the evoked signal still shows non-Gaussian characteristics. In other cases, as for induced responses, the key features of the sources lie in the contrast between two or more alternating states (the *Rest* state versus the *Task* condition). The main role in estimating these types of source is therefore played by the optimisation of a functional constraint index related to the experiment under study, and is

not visible in the global signal probability distribution (insensitive to the time ordering of the data points).

A challenging issue for the proposed approach is when completely new cerebral phenomena are studied, and a priori information is not available. Or, in the case of modelling spontaneous brain activity, where the different alternating states are not induced by an external stimulation, and are therefore unknown. In this direction, integrated studies of intra- and extra-cerebral recordings could perhaps help in estimating a mixture of statistical models of neuronal activity at rest.

Neuroscience has only recently been able to measure cerebral dynamic processes, non invasively, through a variety of imaging technologies, in space and in time. Given the availability of this mass of information, the need for suitable statistical analysis tools is dramatically increased. As the present work set out to show, biostatisticians and neuroscientists find themselves presented with an important and intriguing challenge: by working together to optimise analytical strategies and interpretation of data, they could advance our scientific knowledge of the living brain.

References

1. Del Gratta C, Pizzella V, Tecchio F, Romani G-L. Magnetoencephalography - a non invasive brain imaging method with 1 ms time resolution. *Rep on Progress in Physics* 2001; 64: 1759-1814.
2. Comon P. Independent Component Analysis, a new concept? *Signal Processing* 1994; 36 (3): 287-314.
3. Makeig S, Bell AJ, Jung TP, Sejnowski TJ. Independent Component Analysis of Electroencephalographic Data. *Advances in Neural Information Processing Systems*, 8, MIT Press, 1996: 145-151.
4. Pearson K. On lines and planes of closest fit to systems of points in space. *Philosophical Magazine* 1901; 2: 559-572.
5. Makeig S, Debener S, Onton J, Delorme A. Mining event-related brain dynamics. *Trends Cogn Sci* 2004 May; 8(5):204-10.
6. Barbati G, Sigismondi R, Zappasodi F, Porcaro C, Graziadio S, Valente G, Balsi M, Rossini PM, Tecchio F. Functional Source Separation from Magnetoencephalographic Signals. *Hum Brain Mapp* 2006 Dec; 27 (12): 925-34.
7. Barbati G, Porcaro C, Hadjipapas A, Tecchio F, Pizzella V, Romani GL, Seri S, Barnes GB. Functional Source Separation applied to induced visual gamma activity. *Hum Brain Mapp* Mar 27 2007, Epub ahead of print.
8. Porcaro C, Barbati G, Zappasodi F, Rossini PM, Tecchio F. Hand sensory-motor cortical network assessed by functional source separation. *Hum Brain Mapp* Feb 22, 2007, Epub ahead of print.
9. Tecchio F, Porcaro C, Barbati G, Zappasodi F. Functional source separation and hand cortical representation for a brain-computer interface feature extraction. *J Physiol* 2007; 1 (580): 703-21.
10. Hyvärinen A, Karhunen J, Oja E. *Independent Component Analysis*. New York: Wiley 2001.
11. Cruces-Alvarez S, Castedo-Ribas L, Cichocki A. Robust blind source separation algorithms using cumulants. *Neurocomputing* 2002; 49: 87-118.
12. Barbati G, Porcaro C, Zappasodi F, Rossini PM, Tecchio F. Optimization of ICA approach for artifact identification and removal in MEG signals. *Clinical Neurophysiology* 2004; 115 (5): 1220-32.
13. Peters M, Crowe J, Pieri JF, Quartero H, Hayes-Gill B, James D, Stinstra J, Shakespeare S. Monitoring the foetal heart non-invasively: a review of methods. *J Perinat Med* 2001; 29: 408-16.
14. Lewis MJ. Review of electromagnetic source investigations of the foetal heart. *Med Eng Phys* 2003; 25: 801-10.
15. Hosono T, Kawamata K, Chiba Y, Kandori A, Tsukada K. Prenatal diagnosis of long QT syndrome using magnetocardiography: a case report and review of the literature. *Prenat Diagn* 2002; 22: 198-200.
16. Salustri C, Barbati G, Porcaro C. Foetal Magnetocardiographic Signals Extracted by 'Signal Subspace' Blind Source Separation. *IEEE Trans on Biomedical Engineering* 2005; 52 (6): 1140-1142.
17. Barbati G, Porcaro C, Zappasodi F, Tecchio F. An ICA approach to detect functionally different intra-regional neuronal signals in MEG data, in *Computational Intelligence and Bioinspired Systems Lecture Notes in Computer Science (LNCS 3512)*, pp. 1083-1090, IWANN '05 June 8-10, 2005, Barcelona (Spain).
18. Kirkpatrick S, Gelatt CD Jr, Vecchi MP. Optimization by Simulated Annealing. *Science* 1983; 220 (4598): 671-680.
19. Tecchio F, Rossini PM, Pizzella V, Cassetta E, Romani G-L. Spatial properties and interhemispheric differences of the sensory hand cortical representation: a neuromagnetic study. *Brain Research* 1997; 767: 100-8.
20. Hadjipapas A, Adjamian P, Swettenham JB, Holliday IE, Barnes GR. Stimuli of varying spatial scale induce gamma activity with distinct temporal characteristics in human visual cortex. *Neuroimage* 2007; 135 (2): 518-30.
21. Logothetis NK, Pauls J, Augath M, Trinath T, Oeltermann A. Neurophysiological investigation of the basis of the fMRI signal. *Nature* 2001; 412: 150-157.